Journal of Materials Science and Chemical Engineering, 2022, 10, 24-35
https://www.scirp.org/journal/msce
ISSN Online: 2327-6053
ISSN Print: 2327-6045

Discharge Characteristic of Micro-Arc Oxidation on Aluminum Alloy under the Changing Electrolyte Temperature

Hongwei Yang[1], Xin Wang[1], Zongtao Zhu[2], Ruilin Liu[2*]

[1]CRRC Nanjing Puzhen Co., Ltd., Nanjing, China
[2]School of Materials Science & Engineering, Southwest Jiaotong University, Chengdu, China
Email: *luck_star2009@163.com

How to cite this paper: Yang, H.W., Wang, X., Zhu, Z.T. and Liu, R.L. (2022) Discharge Characteristic of Micro-Arc Oxidation on Aluminum Alloy under the Changing Electrolyte Temperature. *Journal of Materials Science and Chemical Engineering*, **10**, 24-35.
https://doi.org/10.4236/msce.2022.1011003

Received: October 22, 2022
Accepted: November 14, 2022
Published: November 17, 2022

Copyright © 2022 by author(s) and Scientific Research Publishing Inc.
This work is licensed under the Creative Commons Attribution International License (CC BY 4.0).
http://creativecommons.org/licenses/by/4.0/
Open Access

Abstract

The electrolyte temperature has a great influence on the performance of the coating prepared by micro-arc oxidation (MAO). The behavior of MAO discharge in the changing electrolyte temperature has been investigated. Compared to constant electrolyte temperature in conventional MAO process, the process has different discharge characteristics under the changing electrolyte temperature. The amplitude of pulse voltage was detected to study the change of discharge characteristic under the constant-current control of MAO power supply. Three successive discharge stages were differentiated by the variable the pulse voltage versus process time. Since there were significant changes in the sound, the sound signals were acquired and the audio analysis was used to describe the changing of the MAO discharge at different stages. Optical emission spectroscopy (OES) was employed *in situ* to unveil how the micro-discharge changed with the temperature increasing. Scanning electron microscopy (SEM) was used to characterize the morphology of the coatings on 6N01 aluminum alloy prepared by normal process with the constant-temperature control of the MAO electrolyte and by the process under the changing electrolyte temperature. A mode of film growth and micro-discharge was given to describe the effects of the changing electrolyte temperature in the whole MAO process.

Keywords

Micro-arc Oxidation, Aluminum Alloy, Discharge Characteristics, Electrolyte Temperature

1. Introduction

Micro-arc oxidation (MAO) has been an attractive electrochemical process for

the surface modification of aluminum, magnesium and titanium alloys based on the electrical breakdown of the metallic-oxide-coated anode under a significantly high pulse voltage [1]. The properties of MAO coatings are normally related to both electrolytic and electric parameters, such as electrolyte compositions and concentrations [2] [3], applied pulse frequency [4], average current density [5] and treatment time [6].

The electrolyte temperature is one of the major factors that affected the thickness and structures of the MAO coatings. The conventional MAO processes are executed under a constant electrolyte temperature with a cooling system. Mohannad *et al.* [7] studied the microstructures and properties of the 6061 aluminum alloy MAO-coatings in alkali silicate electrolyte temperature from 12.3˚C to 90.5˚C. They found that the increase in electrolyte temperature promoted the participation of the electrolyte in the reaction, which resulted in a thinner, rougher film with larger porosity and more sillimanite and cristobalite phases. Raj *et al.* [8] found that the thickness and growth rate of the films decreased with the increase in electrolyte temperature, which led to worse corrosion behavior.

The cooling system consumes a lot of energy to suppress the increasing electrolyte temperature during traditional MAO treatment. There is another MAO treatment without control of the electrolyte temperature, which means that the electrolyte temperature will keep increasing with the development of MAO exothermal reaction. However, the MAO process without control of the electrolyte temperature has not been demonstrated and reported in publication.

In our previous study, a radical change has been found when the MAO treatment was applied to the electrolyte without cooling system, the accompanying noise was increasing with the electrolyte temperature rising. Until the electrolyte was boiling, the noise suddenly decreased. The properties of the coatings were also different compared to those formed under conventional control mode of the electrolyte temperature [9].

In this case, the MAO treatment was performed on 6N01 aluminum alloy using alkaline-silicate electrolyte under different control modes to systematically investigate the variations in discharge characteristics. The optical emission spectroscopy and acoustic signal were analyzed to understand what happened when the electrolyte-temperature changed.

2. Experimental

The experimental set-up for the study is shown in **Figure 1**. Rectangular specimens (50 × 20 × 3.5 mm^3) of A6N01 aluminum alloy were served as the substrate in this study. The edge of the rectangular coupons was threaded to a pure aluminum bolt to suspend in the electrolyte solution. The A6N01 specimens were grinded with 400-grit emery paper, rinsed in distilled water, ultrasonically cleaned in ethanol for 15 min, and finally dried in air at room temperature. The specimen was immersed in 4 liter electrolyte with 30 g/L of $Na_2SiO_3{\cdot}9H_2O$ and 2 g/L

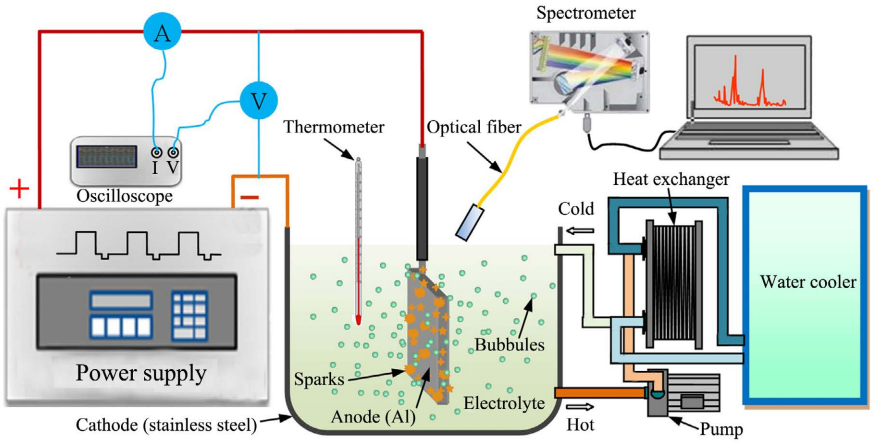

Figure 1. Schematic diagram of the MAO process and measurement system.

KOH, and applied to a pulse voltage with a square waveform at 6 A/dm^2 with a pulse frequency of 600 Hz and a duty cycle of 18%. In the experiments, two different control modes of the electrolyte temperature were used. The 6N01 samples in the solution with the cooling system were treated in the MAO bath at constant 30˚C. Whereas those placed without the cooling system were also treated with monitoring the electrolyte temperature by thermometer, detecting the noise signal by a sound transducer, acquiring the pulse voltage by a oscilloscope (Tektronix TDS 1012C-EDU) and measuring the discharge emission by an optical emission spectrometer (OES, IHR550 Core 3, HORIBA Instruments Inc.). The spectral lines in the range 200 to 820 nm in 0.03 nm steps was used to obtain the emission spectra of the discharge plasma in dark environment.

The thickness of the ceramic coatings that formed on the 6N01 samples was determined at approximately 8 randomly selected places using the eddy flow thickness instrument. The morphology of the surface and the cross-section of the coatings were observed using confocal laser scanning microscopy (CLSM, Nikon A1R+) and a scanning electron microscope (SEM, Zeiss Sigma 300). The average size of the pores of the surface MAO coating was measured by the confocal laser scanning microscopy.

3. Results and Discussion

3.1. Acoustic Signal Analysis of MAO Process

The electrolyte temperature versus process time is shown in Figure 2. The electrolyte temperature without cooling system increased gradually from 12.3˚C till boiling at 90.5˚C, when the processing time was about 1800 s, and then kept almost constant. The electrolyte temperature was around 30˚C in thermostatic control mode. At the beginning of the MAO process without cooling, there was no micro-arc on the surface of the sample due to the anodizing of the Al-alloy substrate at low pulse voltage (see the photo at 10 s in Figure 2). The discharges began to appear a light-white color (the image at 30 s in Figure 2) and then became to an orange-red color at the later stages (the images at 720 s and 1800 s in

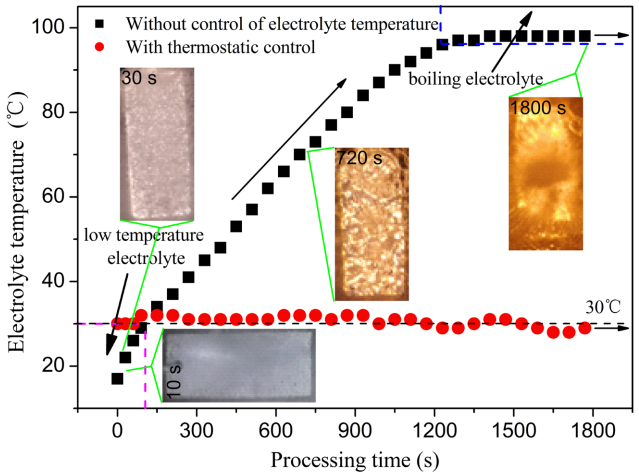

Figure 2. Dependence of different control modes on the electrolyte temperature in the MAO treatment for 30 min.

Figure 2). The amount of the bubbles in the MAO process increased with the electrolyte temperature growing up and the average-size of the bubbles at the beginning stage and the later stage in boiling electrolyte seemed to be smaller than that in intermediate stage.

An interesting phenomenon is that the noise variation of the micro-arc discharge without electrolyte cooling was different compared with that in conventional micro-arc discharge in the electrolyte with constant temperature. Generally, the noise is getting stronger and stronger due the growing discharge voltage applied to the workpiece under the constant-current control mode of power supply. In this case, the noise gradually grew up before the electrolyte boiling, which was similar with traditional MAO process. However, the noise intensity became small when the electrolyte was boiling as shown in the image at 1800 s in Figure 3. The acoustic signals at different time were detected by the sound transducer and oscilloscope and depicted in time domain as shown in Figure 3(a). The amplitude of the acoustic signal had the maximum value at 18 min. In order to analyze the frequency characteristics of the MAO noise, Fast Fourier transform was used to transform the acoustic signals from time domain to frequency domain in Figure 3(b). The characteristic frequencies of the MAO noise were related to the frequency of the pulse voltage applied to the substrate (600 Hz in this case). At the beginning stage of 1-min treatment time, a very low peak at the characteristic frequency of 600 Hz appeared and its amplitude was lower than that of background noise mainly come from the fans in power supply. In intermediate stage at 12 min, there were several characteristic frequencies of 600 Hz, 1225 Hz, 1820 Hz, 2440 Hz and 3664 Hz at 12 min. The peak with the maximum amplitude occurred at 2440 Hz. When the electrode is boiling (30 min), the characteristic frequencies of discharge noise were almost the same as the intermediate state. But the peak with the maximum amplitude of characteristic frequency was located at 600 Hz, which was similar with the beginning state.

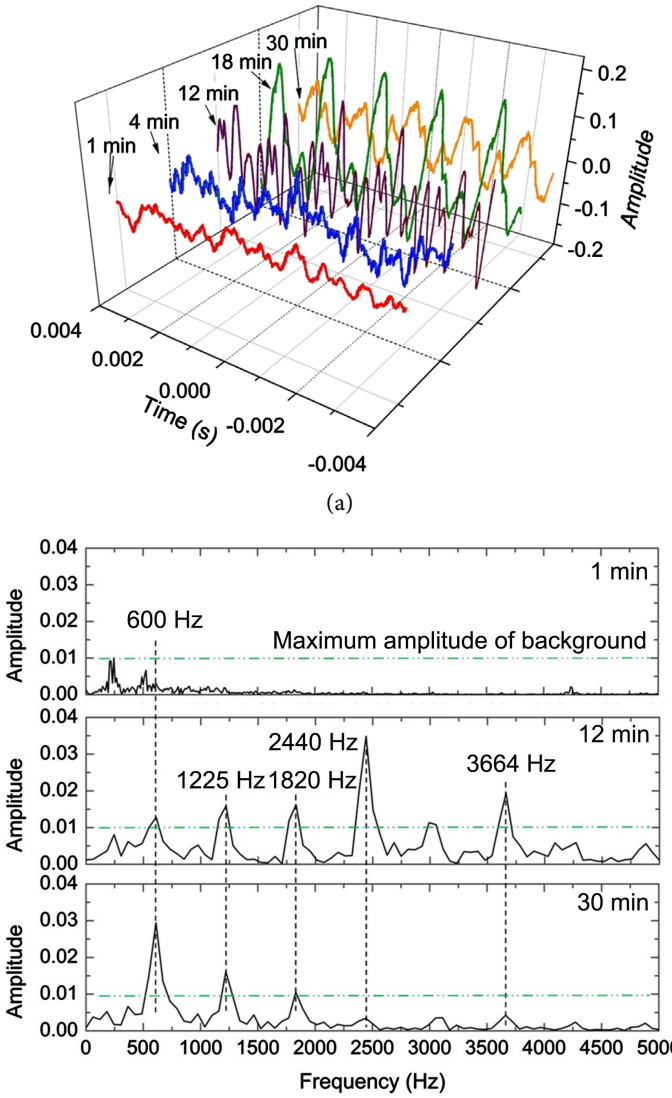

Figure 3. Acoustic signals of the MAO process in (a) time domain and (b) frequency domain without electrolyte cooling.

3.2. Characteristics of the OES Spectra

OES spectra recorded at different stages of MAO process without the electrolyte cooling are shown in **Figure 4**. The spectra were obtained with an integration time of 0.1 s. The presence of the continuous spectrum indicates that large amount of free electrons are generated during MAO processes. Albella *et al.* reported the electron avalanche to associate with the dielectric breakdown during anodization of valve metals and developed a model, in which the primary electronic current of the avalanche was attributed to the electrons released by the electrolyte species in the oxide [10]. **Figure 4(a)** shows that the most salient lines in spectrum belongs to sodium (Na I 588.99 & 589.59 nm) and potassium (K I 766.57 & 769.94 nm), which come from the electrolyte. In constant-current control mode of power supply, the applied voltage grew gradually to sustain breaking

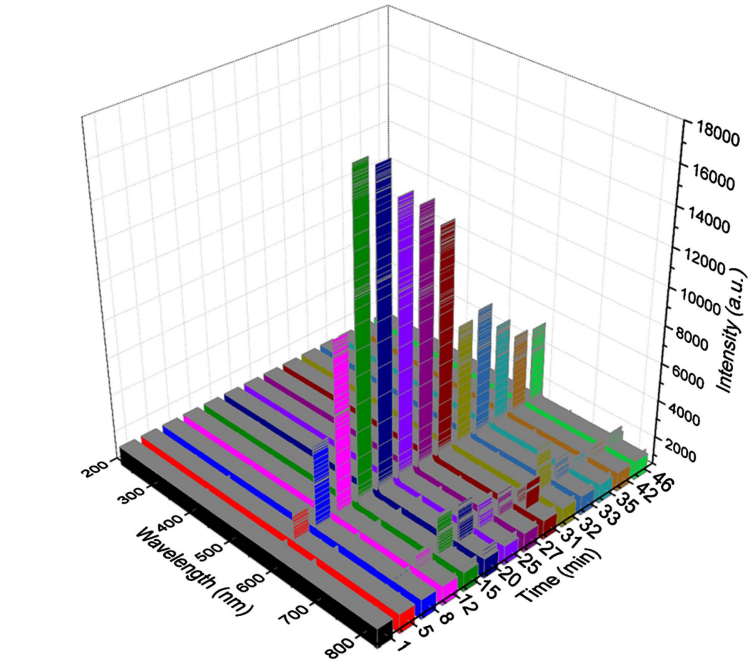

(a)

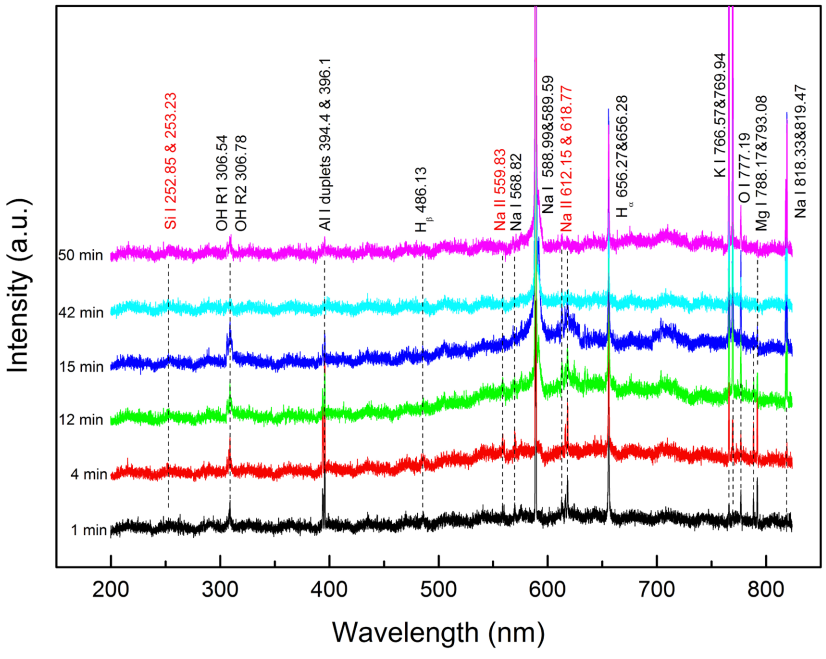

(b)

Figure 4. OES spectra from the MAO process at different treatment time without cooling of the electrolyte: (a) intensity comparison; (b) comparison of the emission lines position.

through the oxide layer to the substrate as powerful arcs, which leads the OES signals of Na and K increased to a higher intensity level from 1 min to 20 min. After the first 20 min, the OES signals declined to a lower intensity level. Especially when the electrolyte was severe boiling after 30 min, the intensity of Na and K lines dropped to a very low level. There were some other species coming

from electrolyte include hydrogen (H_α line at 656.27 & 656.28 nm and H_β 486.13 nm, respectively), OH radical (at 306.54 and 306.78 nm), oxygen (O I line at 777.19 nm), aluminum (Al I duplets 394.4 and 396.1 nm) and magnesium (Mg I line at 788.17 & 793.08 nm), as is shown in **Figure 4(b)**. It was proposed that the high energy electron collision with H_2O, O_2 molecules will generate the H atoms, OH radicals, O atoms [11]. The signals of the Al I and Mg I lines comes from the A6N01 substrate and partly from the anions in the electrolyte, which is existed in the form of $Al(OH)_4^-$ [12]. The intensity-decreasing of Al I and Mg I lines in the spectra indicates that less and less elements of Al and Mg were involved in the oxidation reaction, which was normally unfavorable to the growth of MAO barriers layer. The presence of the OES continuous spectra in the present was similar with traditional MAO process [13]. It seems that the electrolyte without cooling during MAO has little influence on the composition of the active plasma species. But the discharge at the beginning (e.g. at 1 min) is similar spectra with the discharge in boiling electrolyte (e.g. at 50 min) except for the differences in intensity, which means that the most salient lines in spectrum belongs to sodium.

3.3. Three Discharge Stages of MAO Process

The characteristics of the MAO process at a constant current density, which generally consisted of both ionic current and electronic current, were clearly controlled by the pulse voltage response in terms of the process time of 1800 s. Three successive discharge stages I, II and III, which differentiate by the variable trend of the pulse voltage versus process time, were recognized in both electrolyte-temperature control modes, as shown in **Figure 5**. Although the overall trends of the voltage vs. time curve in three stages are similar, the pulse voltage in the electrolyte without cooling was always higher than that in the thermostatic

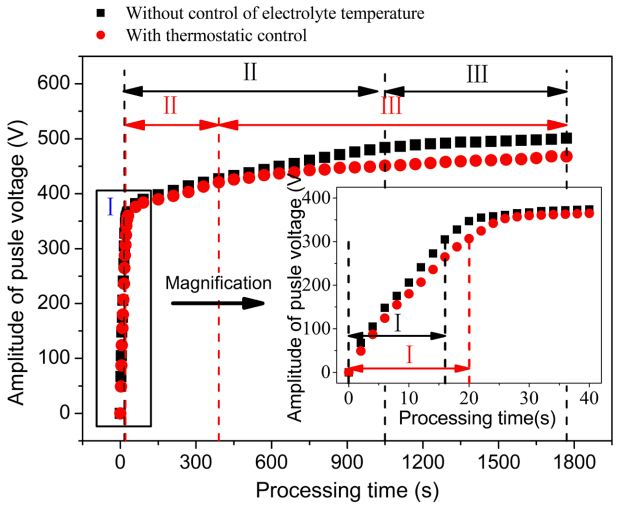

Figure 5. Amplitude of the applied pulse voltage, which was measured from the aluminum samples that were anodized by different control modes of the electrolyte temperature.

electrolyte, and the discharge characteristics in the second and third stages were diverse depending on the control mode of the electrolyte temperature. In the first stage, the curves exhibit breakdown voltages of 305 V and 307 V with the almost fixed slopes of 19 V/s and 15 V/s in 16 s and 20 s of anodizing, respectively, this suggests that the control mode of the electrolyte temperature slightly modified the barrier film characteristics. The breakdown voltages are similar possibly because the breakdown voltage was mainly determined by the substrate alloy with similar electrolyte temperatures at a relatively low level, as shown in Figure 5.

In stage I of MAO without control of electrolyte temperature, compared to the conventional anodizing process, the substrate and metal oxide barriers more slowly dissolved, so the barrier layer has grown faster when the cations and anions transported through the initial alumina film, which was mostly controlled by the ionic current density, which was driven by the electric field [14]. Immediately after the dielectric breakdown occurred on the barrier layer, fine and short-lived sparks were observed, which moved and were homogeneously distributed on the anode surface. Then, the MAO process was considered in the micro-arc oxidation regime, which was simultaneously controlled by the ionic and electric currents, instead of the traditional anodizing regime like the first stage [15].

In the intermediate stage, the pulse voltage continued to successively increase but at a substantially slower rate than before with increasing gas evolution and micro-arc discharges, and the spark color changed from light-white to orange-red. With identical current densities, the consumed MAO electric power in the solution decreased because of the enhanced conductivity of the electrolyte with the increase in solution temperature. Therefore, the desired ionic current to maintain the growth of the coating is decreased because there are more active anions in the solution with increasing temperature. Although the applied voltage to the film increased to a certain extent, the electric field strength per unit volume film evidently decreased because the film rapidly thickened. As a result, the electric current to sustain breakdown and discharge relatively increased, which caused the more intensive motion and higher collision probability of the particles in the plasma. Then, the duration of the instable discharges increased, and the length of this stage obviously increased with the increasing electrolyte temperature.

In the final stage, the pulse voltage reached an almost stable plateau [15]. In MAO process with constant electrolyte temperature, the electric current density became the dominant constituent of the total current density, which implies that the films attained a constant resistance configuration, and no significant increase in anodic voltage was necessary to maintain the current value. With the increase in processing time, even stronger micro discharges and more intensive gas liberation were observed, but the number of sparks decreased, and the sparks became more widely spaced. This result is consistent with a previous study in the literature [16].

However, the discharge characteristics that we observed without electrolyte cooling were notably different from the above discussion. In the entire period of this stage, the electrolyte with a high temperature was boiling, and the solution was rolling around the sample because of the gaseous emission. The micro discharges reverted to being fine, and evenly distributed on the surface of the anodic sample, where the sound of the micro-arc discharges gradually fainted. Hence, this process may be closer to the first stage of the MAO process, which is an enhanced anodizing process because the composition of the electric current rapidly decreased so that the plasma activity was suppressed (see the characteristic frequency of acoustic signals in **Figure 3(b)** and OES spectra in **Figure 4(a)**). Accordingly, over the processing time in the boiling water, the ionic current was again a dominant component of the current density into the oxide conduction band, as in the first period [17]. The film maintained a rapid electrochemical formation with the cations and anions, which actively migrated through the initial alumina film because of the electronic field. That distinction is essential between two control modes of the electrolyte temperature in the final stage.

However, the micro-arc discharge process cannot be steady for a long term in the boiling electrolyte. The sample as the anode was isolated from the electrolyte when large amounts of gas sometimes formed a barrier to inhibit the discharge breakdown and interrupted the circuit, which resulted in the sudden increase in pulse voltage.

3.4. Morphologies and Topographies of MAO Film

Altering the control mode of the electrolyte temperature changes the activity of the anions in the electrolyte and the duration of different stages in the MAO process. As a result, the micro-discharge characteristic is affected, which determines the thermal and chemical conditions during MAO and affects the morphology [18]. To achieve a deeper understanding of the effect of a high-temperature process on the coating growth, the MAO film morphology of samples treated in MAO bath with cooling system at 30˚C and without cooling system was compared.

The surface morphology of the MAO coatings fabricated for different treatments are shown in **Figure 6(a)** and **Figure 6(b)**. Each surface SEM image inserted by the CLSM picture shows the topographies of the surface. The surface topographies comprised of hills and valleys (**Figure 6**). The shapes and dimensions of the micro pores, which were created by discharges, were notably affected by the MAO treatment temperature. Comparing the surface morphologies of the samples that were coated for different temperature in **Figure 6(a)** and **Figure 6(b)**, note that when the MAO treatment was performed to 30 min, many pores turned into elongated oval pores because of the interconnection of the circle pores and the average size of the pores of 9.06 μm. The pores were discharge channels through which cations, anions and the molten materials transporting because of the high gas pressure and strong electric field. Furthermore, the surface

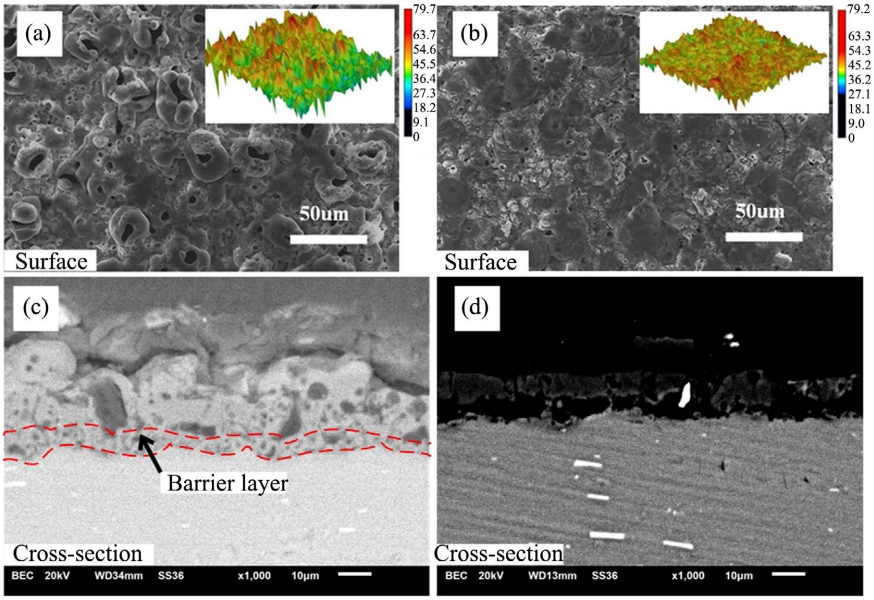

Figure 6. SEM and CLSM images of the MAO coatings: (a) and (c) the sample coated without electrolyte cooling for 30 min; (b) and (d) the sample coated at 30˚C for 30 min.

morphology of the coatings is characterized by a noticeable change with a 30 min treatment at 30˚C, as shown in **Figure 6(b)**. Some pores were sealed, and the micro pore diameter decreased to 2.9 μm, which formed a flatter structure. Nevertheless, the observed surface of the alumina film had many crack defaults. The treatment in constant temperature mode had a notably long period with reasonably intensive discharges, which caused the increase in residual stress in the coating and ultimately the cracking of the coating. The surface topographies of the coating in **Figure 6(b)** show that the surface was much less rough than that in **Figure 6(a)**.

The backscattered micrograph of the cross-sectional features in **Figure 6(c)** and **Figure 6(d)** show the structure of the MAO coatings. The resulting coatings contained porosities because oxygen was trapped in the molten oxides formed by localized discharges [19]. The coating in **Figure 6(c)** was produced for 30 min in the electrolyte without cooling. The coating typically has two layers: a considerable compact barrier layer adjacent to the substrate and a relatively porous layer with discharge channels. The higher-temperature electrolyte possibly penetrated deeper into the growing film during the treatment through the porosities, so that a thicker inner barrier film was formed than that formed in the solution with a constant temperature of 30˚C as shown in **Figure 6(d)**.

4. Conclusions

1) The pulse voltage is always higher in the electrolyte without cooling than that in 30˚C electrolyte. The duration of the second anodization stage is prolonged because of the increased electrolyte temperature and the discharge characteristic changes into the enhanced anodizing process in the boiling electrolyte

at the final stage.

2) The electrolyte without cooling during MAO has little influence on the composition of the active plasma species. The OES spectra at the final stage in boiling electrolyte is similar to the spectra at the first stage except for the differences in intensity, which means that the most salient lines in the spectrum belong to Na I lines.

3) The acoustic signal of micro-arc discharge in electrolyte without cooling has the similar characteristic frequency with the typical value of 600 Hz, which is corresponding to the frequency of pulse voltage applied to the substrate.

4) The MAO process without electrolyte cooling ultimately leads to a thicker and rougher coating on A6N01 aluminum alloy with a respectably thick inner barrier film and elongated oval pores.

Acknowledgements

This work is supported by the Development Projects of Sichuan Province in China (No. 2022YFG0086).

Conflicts of Interest

The authors declare no conflicts of interest regarding the publication of this paper.

References

[1] Yang, Y.H., Feng, G., Gu, Y.H., *et al.* (2021) Analysis on Corrosion of Aluminum-Based Micro-Arc Oxidation Coating. *Anti-Corrosion Methods and Materials*, **68**, 404-412. https://doi.org/10.1108/ACMM-09-2020-2377

[2] Ekin, S., Faiz, M., Yakup, Y., *et al.* (2022) Influence of Electrolyte Compositions and Electrical Parameters on Thermal Properties of Micro-Arc Oxidized AZ91 Alloy. *Journal of Materials and Engineering and Performance*, **31**, 1667-1678. https://doi.org/10.1007/s11665-021-06292-0

[3] Rios, J.M., Quintero, D., Castano, J.G., *et al.* (2022) Effect of EDTA Addition on the Biotribological Properties of Coatings Obtained from PEO on the Ti6Al4V Alloy in a Phosphate-Based Solution. *Surfaces and Interfaces*, **30**, Article ID: 101857. https://doi.org/10.1016/j.surfin.2022.101857

[4] Sobolev, A., Kossenko, A. and Borodianskiy, K. (2019) Study of the Effect of Current Pulse Frequency on Ti-6Al-4V Alloy Coating Formation by Micro Arc Oxidation. *Materials*, **23**, Article No. 3983. https://doi.org/10.3390/ma12233983

[5] Tran, Q.-P., Sun, J.-K., Kuo, Y.-C., *et al.* (2017) Anomalous Layer-Thickening during Micro-Arc Oxidation of 6061Al Alloy. *Journal of Alloys and Compounds*, **697**, 326-332. https://doi.org/10.1016/j.jallcom.2016.11.372

[6] Li, Z.Y., Cai, Z.B., Cui, Y., *et al.* (2019) Effect of Oxidation Time on the Impact Wear of Micro-Arc Oxidation Coating on Aluminum Alloy. *Wear*, **426**, 285-295. https://doi.org/10.1016/j.wear.2019.01.084

[7] Al Bosta, M.M.S. and Ma, K. (2014) Influence of Electrolyte Temperature on Properties and Infrared Emissivity of MAO Ceramic Coating on 6061 Aluminum Alloy. *Infrared Physics & Technology*, **67**, 63-72. https://doi.org/10.1016/j.infrared.2014.07.009

[8] Raj, V. and Mubarak Ali, M. (2009) Formation of Ceramic Alumina Nanocomposite Coatings on Aluminium for Enhanced Corrosion Resistance. *Journal of Materials Processing Technology*, **209**, 5341-5352. https://doi.org/10.1016/j.jmatprotec.2009.04.004

[9] Wang, X.F., Zhu, Z.T., Li, Y.X. and Chen, H. (2018) Characterization of Micro-Arc Oxidation Coatings on 6N01 Aluminum Alloy under Different Electrolyte Temperature Control Modes. *Journal of Materials Engineering and Performance*, **27**, 1890-1897. https://doi.org/10.1007/s11665-018-3313-y

[10] Albella, J.M., Montero, I. and Martinez-Duart, J.M. (1987) A Theory of Avalanche Breakdown during Anodic Oxidation. *Electrochimica Acta*, **32**, 255-258. https://doi.org/10.1016/0013-4686(87)85032-6

[11] Wang, L., Chen, L., Yan, Z. and Fu, W. (2010) Optical Emission Spectroscopy Studies of Discharge Mechanism and Plasma Characteristics during Plasma Electrolytic Oxidation of Magnesium in Different Electrolytes. *Surface and Coatings Technology*, **205**, 1651-1658. https://doi.org/10.1016/j.surfcoat.2010.10.022

[12] Cheng, Y., Mao, M., Cao, J. and Peng, Z. (2014) Plasma Electrolytic Oxidation of an Al-Cu-Li Alloy in Alkaline Aluminate Electrolytes: A Competition between Growth and Dissolution for the Initial Ultra-Thin Films. *Electrochimica Acta*, **138**, 417-429. https://doi.org/10.1016/j.electacta.2014.06.122

[13] Cheng, Y.L., Wang, T., Li, S.X., Cheng, Y.L., Cao, J.H. and Xie, H.J. (2017) The Effects of Anion Deposition and Negative Pulse on the Behaviours of Plasma Electrolytic Oxidation (PEO)—A Systematic study of the PEO of a Zirlo Alloy in Aluminate Electrolytes. *Electrochimica Acta*, **25**, 47-68. https://doi.org/10.1016/j.electacta.2016.12.115

[14] Sarvan, M., Radić-Perić, J., Kasalica, B., Belča, I., Stojadinović, S. and Perić, M. (2014) Investigation of Long-Duration Plasma Electrolytic Oxidation of Aluminum by Means of Optical Spectroscopy. *Surface and Coatings Technology*, **254**, 270-276. https://doi.org/10.1016/j.surfcoat.2014.06.029

[15] Veys-Renaux, D. and Rocca, E. (2015) Initial Stages of Multi-Phased Aluminium Alloys Anodizing by MAO: Micro-Arc Conditions and Electrochemical Behavior. *Journal of Solid State Electrochemistry*, **19**, 3121-3129. https://doi.org/10.1007/s10008-015-2935-3

[16] Fattah-alhosseini, A. and Sabaghi Joni, M. (2015) Effect of KOH Concentration on the Microstructure and Electrochemical Properties of MAO-Coated Mg Alloy AZ31B. *Journal of Materials Engineering and Performance*, **24**, 3444-3452. https://doi.org/10.1007/s11665-015-1645-4

[17] Venkateswarlu, K., Rameshbabu, N., Sreekanth, D., *et al.* (2013) Role of Electrolyte Chemistry on Electronic and *in Vitro* Electrochemical Properties of Micro-Arc Oxidized Titania Films on Cp Ti. *Electrochimica Acta*, **105**, 468-480. https://doi.org/10.1016/j.electacta.2013.05.032

[18] Dehnavi, V., Shoesmith, D.W., Luan, B.L., Yari, M., Liu, X.Y. and Rohani, S. (2015) Corrosion Properties of Plasma Electrolytic Oxidation Coatings on an Aluminium Alloy—The Effect of the PEO Process Stage. *Materials Chemistry and Physics*, **161**, 49-58. https://doi.org/10.1016/j.matchemphys.2015.04.058

[19] Zehra, T. and Kaseem, M. (2022) Recent Advances in Surface Modification of Plasma Electrolytic Oxidation Coatings Treated by Non-Biodegradable Polymers. *Journal of Molecular Liquids*, **365**, Article ID: 120091. https://doi.org/10.1016/j.molliq.2022.120091